

Water as Buffer Material for Gold Nanocluster Growth

Elad Gross, Yonatan Horowitz, and Micha Asscher*

Department of Physical Chemistry and the Farkas Center for Light-Induced Processes,
The Hebrew University of Jerusalem, Jerusalem 91904, Israel

Received May 10, 2005. In Final Form: July 18, 2005

Water molecules adsorbed on SiO₂/Si(100) at 140 K to form amorphous solid water (ASW) layers were utilized as a buffer for assisting the growth of gold nanoclusters. It was shown that the average height and diameter of the clusters deposited on the silicon oxide substrate following the buffer annealing/desorption increase as the buffer layer becomes thicker and as more gold is deposited. The clusters' height and diameter were determined by tapping mode AFM and high-resolution SEM imaging, respectively. Typical heights were between 0.5 and 4.5 nm, and the diameters were in the range of 3–9 nm for ASW layer thickness of 7–100 ML and gold deposition in the range of 0.2–1.2 Å. The density of the clusters decreased from 65×10^{10} to 8×10^{10} cm⁻² in the same buffer layer thickness range. Significantly different morphology of the clusters is obtained when compared to those formed by direct deposition of gold on the silicon oxide surface and to those grown on top of Xe as buffer material.

1. Introduction

Metallic clusters supported on oxide substrates are the basis for industrial heterogeneous catalysis.^{1–4} Gold nanoclusters held on oxide substrates were recently found to be active as an efficient catalyst for CO oxidation, despite the inert behavior of gold as a bulk material. The highest catalytic activity for CO oxidation was demonstrated to be limited to gold clusters 3 ± 1 nm in size.^{5–8} These observations nicely demonstrate the extreme sensitivity of the catalytic action to the catalysts' particle size.

Vacuum deposition of metallic clusters on bare oxide substrates has been a typical approach in model heterogeneous catalysis studies. Clusters grow via metal atom diffusion and aggregation on the substrate, whereas their density and dimensions are dictated by the substrate's temperature, flux of incoming atoms and the total amount of evaporated metal.⁹ The nature of the support is significant because the diffusion is governed by the surface free energy, metal-to-oxide strength of interaction and probably most important, the surface density of defects and imperfections.^{1–4,10–18} Clusters grown via a direct

evaporation procedure are characterized by a relatively narrow size distribution^{10,11,14,18} and aspect ratio (height-to-diameter ratio) that is typically less than 0.3.

Another method for the growth of clusters has been introduced by Huang et al. using xenon as an inert buffer layer.¹⁹ Evaporated metal on top of the xenon layer was subsequently deposited on a substrate held at 20 K. As the xenon layer desorbs following slow annealing, the metallic clusters coalesce and grow in size via a buffer layer assisted growth (BLAG) mechanism. BLAG-generated density and dimensions of clusters are controlled by the buffer layer thickness and amount of evaporated metal.^{19–23} Employing the BLAG approach eliminates much of the dependence of the clusters' shape on the chemical nature and properties of the substrate. Other metals and semiconductor clusters were recently reported to grow via BLAG employing noble atoms as well as molecular buffers such as CO and ice as the buffer materials.^{21,24,25}

In this article, we demonstrate that amorphous solid water layers function as an efficient buffer material for the growth of metallic clusters. Native silicon oxide, SiO₂/Si(100), was chosen as the substrate in this study as a model for silica supports in industrial applications. This substrate is, however, far smoother than the industrial oxide, as shown below (Figure 1E). An analysis of cluster size and density has been performed by employing atomic force microscopy (AFM) and high-resolution scanning electron microscopy (HR-SEM) measurements.

We demonstrate that the height of clusters and the density are power law-dependent on the water layer

* To whom correspondence should be addressed. E-mail: asscher@fh.huji.ac.il. Tel: +972-2-6518033. Fax: +972-2-6525037.

- (1) Campbell, C. T. *Surf. Sci. Rep.* **1997**, *27*, 1.
- (2) Henry, C. R. *Surf. Sci. Rep.* **1998**, *31*, 231.
- (3) Bäumer, M.; Freund, H. *J. Prog. Surf. Sci.* **1999**, *61*, 127.
- (4) Goodman, D. W. *J. Catal.* **2003**, *216*, 213.
- (5) Valden, M.; Lai, X.; Goodman, D. W. *Science* **1998**, *281*, 1647.
- (6) Chusuei, C. C.; Lai, X.; Luo, K.; Goodman, D. W. *Top. Catal.* **2001**, *14*, 71.
- (7) Choudhary, T. V.; Goodman, D. W. *Top. Catal.* **2002**, *21*, 25.
- (8) Haruta, M. *Catal. Today* **1997**, *36*, 153.
- (9) Wulfhekel, W.; Lipkin, N. N.; Kliewer, J.; Rosenfeld, G.; Jorritsma, L. C.; Poelsema, B.; Comsa, G. *Surf. Sci.* **1996**, *348*, 227.
- (10) Xu, C.; Oh, W. S.; Liu, G.; Kim, D. Y.; Goodman, D. W. *J. Vac. Sci. Technol., A* **1997**, *15*, 1261.
- (11) Lai, X.; St Clair, T. P.; Valden, M.; Goodman, D. W. *Prog. Surf. Sci.* **1998**, *59*, 25.
- (12) Luo, K.; Kim, D. Y.; Goodman, D. W. *J. Mol. Catal. A: Chem.* **2001**, *167*, 191.
- (13) Min, B. K.; Santra, A. K.; Goodman, D. W. *J. Vac. Sci. Technol., B* **2003**, *21*, 2319.
- (14) Kolmakov, A.; Goodman, D. W. *Chem. Rec.* **2002**, *2*, 446.
- (15) Min, B. K.; Wallace, W. T.; Santra, A. K.; Goodman, D. W. *J. Phys. Chem. B* **2004**, *108*, 16339.
- (16) Zhang, L.; Cosandey, F.; Persaud, R.; Madey, T. E. *Surf. Sci.* **1999**, *439*, 73.
- (17) Schmidt, A. A.; Eggers, H.; Herwig, K.; Anton, R. *Surf. Sci.* **1996**, *349*, 301.

(18) Chen, D. A.; Bartelt, M. C.; Seutter, S. M.; McCarty, K. F. *Surf. Sci.* **2000**, *464*, L708.

(19) Huang, L.; Chey, S. J.; Weaver, J. H. *Phys. Rev. Lett.* **1998**, *80*, 4095.

(20) Haley, C.; Weaver, J. H. *Surf. Sci.* **2002**, *518*, 243.

(21) (a) Antonov, V. N.; Palmer, J. S.; Bhatti, A. S.; Weaver, J. H. *Phys. Rev. B* **2003**, *68*, 205418. (b) Antonov V. N.; Weaver, J. H. *Surf. Sci.* **2003**, *526*, 97.

(22) Kerner, G.; Horowitz, Y.; Asscher, M. *J. Phys. Chem B* **2005**, *109*, 4545.

(23) Waddill, G. D.; Vitomirov, I. M.; Aldao, C. M.; Anderson, S. G.; Capasso, C.; Weaver, J. H.; Liliental-Weber, Z. *Phys. Rev. B* **1990**, *41*, 5293.

(24) Yan, X.-M.; Ni, J.; Robbins, M.; Park, H. J.; Zhao, W.; White, J. M. *J. Nanopart. Res.* **2002**, *4*, 525.

(25) Yoo, K.; Li, A.-P.; Zhang, Z.; Weitering, H. H.; Flack, F.; Lagally, M. G.; Wendelken, J. F. *Surf. Sci.* **2003**, *546*, L803.

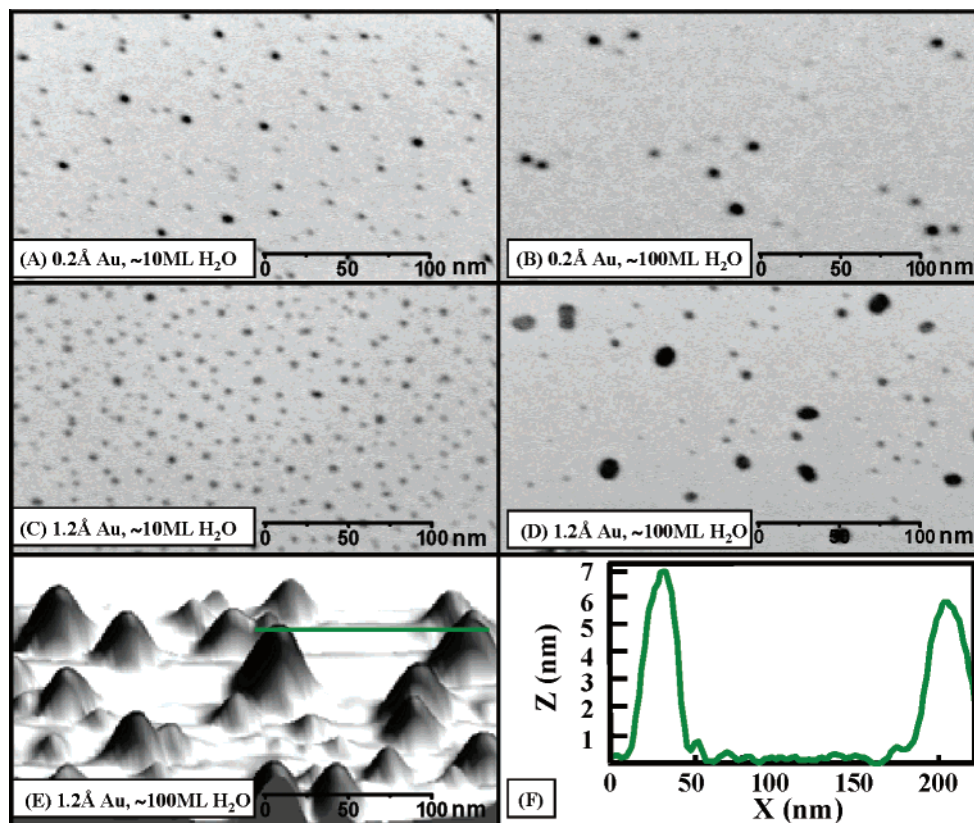


Figure 1. Water buffer layer assistance-grown (BLAG) gold clusters on a SiO₂/Si(100) substrate held at 140 K. (A–D) HR-SEM images taken ex situ at room temperature. The dark spots are gold clusters. The SEM images were used to determine the diameter of the clusters. (E) Three-dimensional AFM image taken ex situ at room temperature. The AFM images were used to determine the height of the clusters. Buffer layer thicknesses and the amount of deposited gold are indicated. (F) Line-scan profile of the clusters and substrate in E.

thickness. Comparing the BLAG results with those obtained when clusters are grown via direct deposition on the SiO₂/Si(100) substrate with no buffer layer assistance has indicated that the BLAG method leads to the formation of more-spherical 3D clusters at lower density. Comparison between Xe and H₂O as buffer materials has revealed an important difference in the density of clusters, which is attributed to the order-of-magnitude larger heat capacity of water compared to that of Xe.

2. Experimental Section

The SiO₂/Si(100) samples were prepared at a typical base pressure of 5×10^{-9} Torr. Square pieces 2×2 cm² cut from an n-type Si(100) wafer, 10^{-2} Ω/cm, were attached to a liquid-nitrogen dewar via two tantalum foils, which were spot welded to copper feedthroughs. A W26%Re–W5%Re thermocouple was spot welded to the tantalum foil. The temperature difference between the tantalum foil and the sample was calibrated by temperature programmed desorption (TPD) measurements of multilayer water. After annealing the sample at 700 K, triple-distilled H₂O molecules were introduced by backfilling the UHV chamber while the sample temperature was kept at 140 K. Sample cleanliness was verified by XPS measurements performed in another chamber to ensure the cleanliness of the silicon oxide following the annealing procedure. Water exposures were determined by backfilling the chamber to 1×10^{-6} Torr for different time intervals equivalent to water exposures of 7–100 langmuirs (L) ($1 \text{ L} = 10^{-6} \text{ Torr}\cdot\text{s}$). The sticking probability of water at 140 K was assumed to be unity, and the exposure of 1 L was considered to be equivalent to 1 ML of H₂O on the SiO₂/Si(100) substrate.²⁶

Gold atoms were evaporated onto the water buffer layer in vacuum. Resistively heated tungsten wire (0.25 mm diameter)

wrapped around a 1-mm-diameter Au wire (99.99% pure) was the metal deposition source. Gold flux was calibrated by utilizing an in-situ quartz microbalance employing deposition rates of 0.01–0.02 Å/s.

Under our experimental conditions with a substrate temperature of 140 K, the water buffer layer has the compact structure of amorphous solid water (ASW).²⁶ Because of the weak Au–H₂O interaction, small gold clusters are formed upon deposition on top of the ASW surface.

The sample was heated to 300 K at a rate of 2 K/s after the metal deposition step to remove the water layer. Coalescence and growth of the gold nanoclusters during the buffer layer desorption result in the eventual deposition of the clusters on the SiO₂/Si(100) substrate.

The sample was then removed from the vacuum chamber to (ex-situ) image the metallic clusters by AFM and HR-SEM at room temperature. The height of the clusters was determined by tapping mode AFM measurements. Light tapping scan mode was employed throughout to reduce to a minimum height distortion effects. As a result, we found no evidence for any dependence of height on the tip properties (force constant and resonance frequency).²⁷ Because of tip limitations in the utilization of AFM for the determination of nanoclusters' lateral dimensions, we chose to determine the cluster diameter by HR-SEM having a manufacturer specification of 1.5 nm as its lateral resolution. Special care was taken to avoid any influence of the electron beam on the shape of clusters while measuring. Combining the information from the two complementary imaging techniques makes it possible to determine the shape of the clusters in terms of the average diameter and height or their aspect ratio defined as the height/diameter ratio. The stability of the gold clusters against exposure to air at atmospheric pressure was checked.²² A change in neither the density of the clusters nor in their size was observed after exposure to air for several weeks.

(26) Brown, D. E.; George, S. M.; Huang, C.; Wong, E. K. L.; Rider, K. B.; Smith, R. S.; Kay, B. D. *J. Phys. Chem.* **1996**, *100*, 4988.

(27) Ebenstein, Y.; Nahum, E.; Banin, U. *Nano Lett.* **2002**, *2*, 945.

3. Results and Discussion

3.1. Cluster Growth via the Water Buffer Layer.

The main goal of this research has been to replace the inert and weakly bound Xe^{19–21} by a molecular buffer material having internal degrees of freedom and therefore a higher heat capacity, such as that of water, to assist in the controlled growth of metallic nanoclusters on a solid substrate.

Different amounts of gold were evaporated (amount of evaporated gold = $D_{(g)}$) on different water layer thicknesses (water layer thickness = θ) deposited on a SiO₂/Si(100) substrate held at 140 K. Figure 1 shows HR-SEM images of four different gold/water buffer/SiO₂ samples. For $D_{(g)} = 0.2 \text{ \AA}$ and $\theta = 10 \text{ ML}$ (Figure 1A), the density of clusters (density of clusters = $\langle n \rangle$) was $30 \times 10^{10} \text{ cm}^{-2}$ as extracted from scan images taken from different areas. The average height of clusters (average height of clusters = $\langle h \rangle$) for the same sample was 0.5 nm (as analyzed by AFM measurements). The effect of the buffer layer thickness is demonstrated when $D_{(g)}$ is kept the same at 0.2 Å and θ is increased to 100 ML (Figure 1(B)); $\langle n \rangle$ was subsequently reduced to $8 \times 10^{10} \text{ cm}^{-2}$, whereas $\langle h \rangle$ increased to 2 nm. The effect of the gold dosage can be seen when $D_{(g)} = 1.2 \text{ \AA}$ and $\theta = 10 \text{ ML}$ (Figure 1C); $\langle n \rangle$ increased by 100% to $60 \times 10^{10} \text{ cm}^{-2}$, whereas $\langle h \rangle$ has increased to 2.1 nm, which is a factor of 4 with respect to the conditions in Figure 1A. Clusters formed by $D_{(g)} = 1.2 \text{ \AA}$ and $\theta = 100 \text{ ML}$ (Figure 1D) were less dense with $\langle n \rangle = 10 \times 10^{10} \text{ cm}^{-2}$, but a significant increase in average height to $\langle h \rangle = 4.5 \text{ nm}$ has been recorded. The formation of large clusters is often associated with the aggregation of several small clusters into a larger one, without fusion into a single large cluster as can be seen in the SEM image in Figure 1D. These aggregates are thermally stable following annealing in vacuum up to 400 K.

A comparison of the two borderline cases shown in Figure 1A–D demonstrates that by changing the initial parameters of the BLAG method (n) could be reduced by 7 fold and $\langle h \rangle$ increased by an order of magnitude. These images demonstrate the strong dependence of the clusters' dimensions and density on θ and $D_{(g)}$, the two variables that dominate BLAG.^{19–22} A further examination of Figure 1A–D reveals that the width of the size distribution of clusters increases along with the dimensions of the clusters. When a thin buffer layer is used, uniform clusters with a relatively narrow size distribution are grown (Figure 1A and C), unlike the case of thick buffer layers (Figure 1B and D) where relatively wide size distributions characterize the growth of clusters.

Cluster densities extracted from both SEM and AFM images (Figure 1D and E, respectively) taken from the same substrate are almost identical. Nevertheless, the diameter of clusters shown in the AFM image in Figure 1E looks significantly larger than the diameter in the SEM image (Figure 1D). This phenomenon is attributed to a tip convolution effect.²⁷ In Figure 1F, a typical line scan provides the height profile of clusters as obtained by AFM. It also emphasizes the contrast with the smooth native SiO₂ substrate.

3.2. Density of Clusters. Varying the initial parameters of the BLAG method changes $\langle n \rangle$ values remarkably when the buffer material is Xe.^{19–22} We tested the dependence of $\langle n \rangle$ on θ and $D_{(g)}$ (Figure 2) with water as the buffer material. Three different $D_{(g)}$ values for different water thicknesses resulted in $\langle n \rangle$ in the range of 8×10^{10} to $60 \times 10^{10} \text{ cm}^{-2}$. We note that as $D_{(g)}$ diminished and θ increased, $\langle n \rangle$ decreased. Because the metal deposition time is longer (larger values of $D_{(g)}$), the density of the

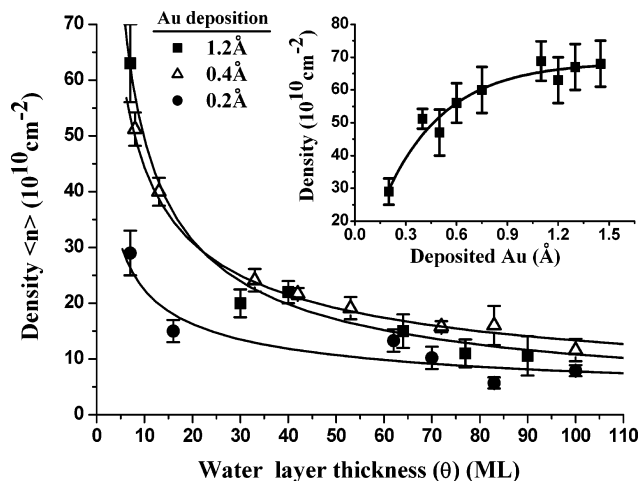


Figure 2. Average density of clusters ($\langle n \rangle$) plotted as a function of buffer layer thickness (θ) for three different amounts of evaporated gold, determined by a quartz microbalance. The power law dependence (solid lines) follows the expression $\langle n \rangle \propto \theta^Z$, with $Z = -0.45, -0.5,$ and -0.6 for 0.2, 0.4, and 1.2 Å of evaporated gold, respectively. (Inset) Density of clusters as a function of the amount of gold deposited on a fixed buffer layer thickness of 7 ML of H₂O.

initial seeds of metallic clusters on top of the buffer is expected to grow; therefore, $\langle n \rangle$ will also increase after water desorption. However, as θ increases, $\langle n \rangle$ should decrease because the coalescence and aggregation process of the small clusters is more effective. A power law dependence of $\langle n \rangle$ on θ was found, $\langle n \rangle \propto \theta^Z$, where $Z = -0.45, -0.5,$ and -0.6 for $D_{(g)} = 0.2, 0.4,$ and 1.2 \AA , respectively.²⁰ Z and $D_{(g)}$ are only slightly correlated with each other.

The average cluster density $\langle n \rangle$ reached its saturation value for layer thickness $\theta > 80 \text{ ML}$ near $\sim 10 \times 10^{10} \text{ cm}^{-2}$. Apparently, above 80 ML the size of the clusters formed in the initial stage of water evaporation limits their mobility or diffusion enough to prevent further aggregation.¹⁹ Another manifestation of the density saturation can be demonstrated by doubling $D_{(g)}$ from 0.2 to 0.4 Å; $\langle n \rangle$ (for a constant θ value of 7 ML) increased by 70%. However, when $D_{(g)}$ was tripled from 0.4 to 1.2 Å under similar θ values, no significant changes in $\langle n \rangle$ were observed.

To quantify the $\langle n \rangle$ dependence on $D_{(g)}$, we have conducted experiments in which different amounts of gold were evaporated on top of 7 ML of water (Figure 2, inset). It can be concluded that $\langle n \rangle$ grows along with $D_{(g)}$ at small $D_{(g)}$ values until it approaches saturation (at $D_{(g)} \approx 1 \text{ \AA}$). At this point, any additional atom that hits the ice surface has a short diffusion length to the nearest cluster. Consequently, the size of the clusters increases, whereas their density does not change as long as θ is kept constant.^{20,24} In a recent report, Yan et al.²⁴ have shown that the evaporation of 3.5 Å of Ag on 7 ML of H₂O over a HfO₂ substrate resulted in cluster formation at a density of $2 \times 10^{10} \text{ cm}^{-2}$. This report supports our observations that above a given amount of evaporated metal on top of the buffer layer $\langle n \rangle$ saturates and even somewhat decreases. This may be explained by the partial percolation of neighboring clusters on top of the buffer layer prior to its desorption.²⁰

3.3. Height of Clusters. Next we have attempted to assess the dependence of the average height of clusters ($\langle h \rangle$) on the initial BLAG parameters. We measured the $\langle h \rangle$ dependence on θ for different values of $D_{(g)}$ (Figure 3) and found that $\langle h \rangle$ increases together with $D_{(g)}$ and θ . A

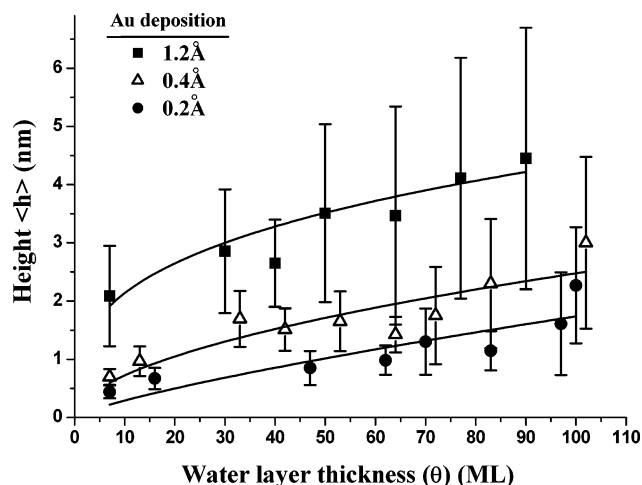


Figure 3. Average height ($\langle h \rangle$) of the gold clusters as a function of buffer layer thickness (θ) plotted for three different amounts of evaporated gold. The power law dependence (solid lines) follows the expression $\langle h \rangle \propto \theta^Z$, with $Z = 0.3, 0.53,$ and 0.8 for $0.2, 0.4,$ and 1.2 \AA of evaporated gold, respectively. Error bars reflect ± 1 standard deviation.

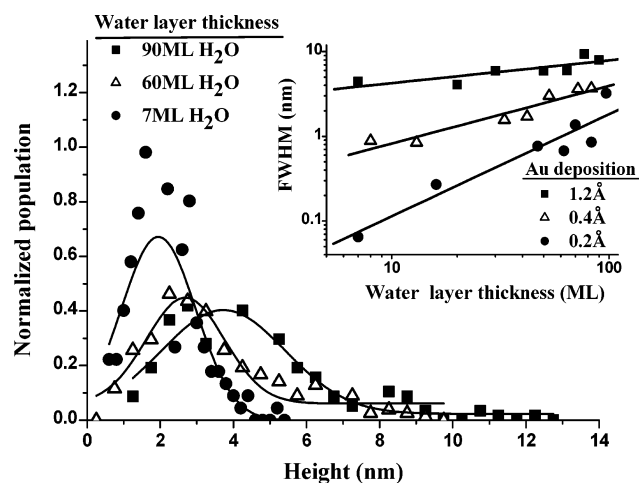


Figure 4. Normalized height distributions and their Gaussian fit for clusters grown following the deposition of 1.2 \AA of gold on top of the indicated ASW layer thicknesses. Full width at half-maximum (fwhm) values were obtained from the Gaussian profiles. fwhm values of $4.3, 6,$ and 8 nm are correlated with water buffer layer thicknesses of $7, 60,$ and 100 ML , respectively. (Inset) Logarithmic plot of fwhm as a function of H₂O layer thickness for the indicated amounts of deposited gold.

power law dependence of $\langle h \rangle$ on θ was found,²⁰ $\langle h \rangle \propto \theta^Z$, where $Z = 0.3, 0.53,$ and 0.8 for $D_{(g)} = 0.2, 0.4,$ and 1.2 \AA , respectively. Unlike the dependence of $\langle n \rangle$ on $D_{(g)}$ and θ , the power law correlating $\langle h \rangle$ with $D_{(g)}$ and θ reveals a monotonic and rather significant increase in Z with $D_{(g)}$.

Although saturation values for the density of clusters could be defined, the height of the clusters never reached saturation in the ranges of $D_{(g)}$ and θ studied here. The heights of clusters continue to increase, even when almost no further coalescence takes place, as one approaches the density saturation.

A correlation was found between the width of the cluster size distribution and $\langle h \rangle$. As could be expected, the distribution becomes wider as $\langle h \rangle$ increases.¹⁹ To demonstrate the size variation of the clusters, we plotted three normalized height distributions together with a respective Gaussian fit for clusters made by different θ values but the same $D_{(g)}$ (Figure 4). Height distributions are expressed in terms of Gaussian full width at half-maximum (fwhm)

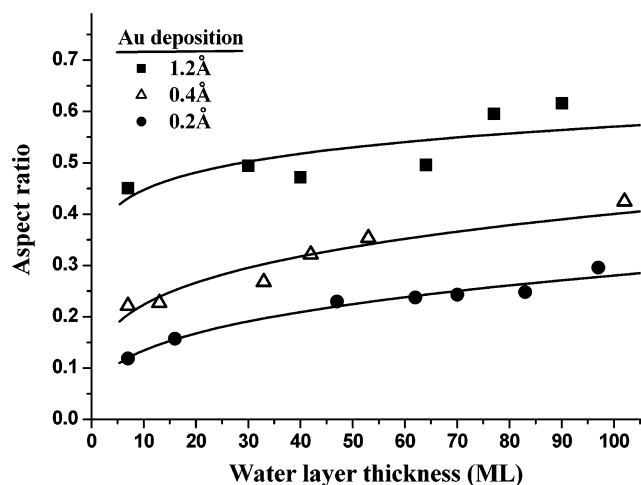


Figure 5. Aspect ratio (height/diameter) of clusters as determined by tapping mode AFM and HR-SEM plotted vs water layer thickness for the indicated amounts of evaporated gold as determined by a quartz microbalance.

values. The fwhm values of these three height distributions are $4.3, 6,$ and 8 nm for $\theta = 7, 60,$ and 90 ML , respectively, all at $D_{(g)} = 1.2 \text{ \AA}$. The fwhm of height distributions was plotted versus θ for different values of $D_{(g)}$ to better understand the role of deposition flux in determining the size of the clusters (Figure 4, inset). fwhm values increase as a result of increasing $D_{(g)}$ and are not only due to thicker buffer layers (θ). Similar results were reported by Huang et al.¹⁹ We also note that the rate at which fwhm values grow gradually slows down as $D_{(g)}$ increases.

Figure 4 further demonstrates that height distributions of clusters are less symmetric in the case of the smaller clusters. This phenomenon can be rationalized by the fact that in order to form higher clusters coalescence or aggregation of two or more small clusters must occur. The coalescence process depletes small clusters from the distribution in favor of larger ones, which results in asymmetric fwhm distribution profiles. These results are in agreement with data analyzed by Huang et al.¹⁹

3.4. Diameter of Clusters: HR-SEM Measurements. HR-SEM images were taken to verify the diameter of clusters. AFM measurements are not accurate enough to determine the lateral dimensions of clusters. This is due to distortions caused by the AFM tip profile (15 nm maximum radius), resulting in significantly larger diameters than the actual values with errors up to 100% .²⁷ In contrast, HR-SEM is capable of determining diameters to within 20% accuracy for clusters larger than 2 nm in diameter.

A combination of height analysis (monitored by AFM) and the diameter of clusters (determined by HR-SEM) allows a better estimate of the actual size of clusters. Variations of the aspect ratio, defined as the ratio of the clusters' average height to their diameter, are shown in Figure 5 as a function of θ for three different values of $D_{(g)}$. It is assumed that clusters are attached to the surface as half (filled) spheres, with their basis toward the surface.¹⁹

It can be seen that as the buffer layer thickness grows, the morphology of clusters changes. For the case of thin ASW layers (low θ values) at $D_{(g)} = 1.2 \text{ \AA}$, oblate clusters are formed on the substrate, in agreement with results reported by Yan et al.²⁴ for Ag particles on the HfO₂ surface. At $\theta > 40 \text{ ML}$, the clusters gradually become closer in shape to half spheres. The aspect ratio of clusters is also affected by $D_{(g)}$, where more flattened clusters with a lower aspect ratio are typical for $D_{(g)} < 0.5 \text{ \AA}$.

As stated above, the aspect ratio of the deposited gold clusters increases with the buffer layer thickness. This can be rationalized as arising from the fact that the BLAG method is initiated by small metallic clusters (seeds) growing on top of the ASW layer. These clusters diffuse through the desorbing water molecules toward the surface during the annealing step. When the buffer layer thickness is small, the aggregation process during water desorption is negligible; therefore, the shape and size of clusters on the surface closely reflect their morphology on top of the ASW surface.¹⁹ Clusters on top of the ASW layer grow via 2D diffusion and coalescence of the small seed clusters. This leads to a relatively low aspect ratio. As the buffer layer becomes thicker, 3D diffusion and aggregation processes lead to higher aspect ratios. It is interesting that the results reported by Yan et al.²⁴ are based on an interpretation of AFM images. These authors conclude that Ag clusters grown via BLAG with H₂O as the buffer layer on a HfO₂ substrate have a rather nonsymmetric distribution of cluster diameters. This distribution is characterized by an abrupt cutoff for larger cluster populations. In contrast, analyzing our results using the HR-SEM data (not shown) and AFM (Figure 4) suggests that the distributions of cluster diameters and heights are quite symmetric, in particular for large average size clusters. One should, however, take into account the limited SEM resolution that may contribute to a certain level of asymmetry within our distributions of diameters, in particular at the smaller size end. Small clusters diffuse faster than larger clusters at a given temperature;²² therefore, small clusters may coalesce and aggregate to form larger clusters. This Ostwald ripening-like process would lead to somewhat nonsymmetrical size distributions, particularly for small average diameters.²¹

The number of atoms contained in each cluster can be estimated on the basis of the AFM and HR-SEM measurements. The number of gold atoms in each of the BLAG-prepared flattened clusters ranges roughly from 200 (3 nm diameter) to 50 000 (8 nm diameter), as extracted from θ and $D_{(g)}$. Cluster sizes deduced from such estimates are in good agreement with the amount of gold evaporated on top of the water layer and calibrated by the in-situ quartz microbalance monitor.

3.5. Xe versus H₂O as a Buffer Material. The typical buffer material used extensively by Weaver and co-workers in their early study of the BLAG method was xenon,^{19–21,23} which differ significantly from water because it is atomic, much heavier, and chemically inert. In addition, the heat capacity of ice is more than 10 times higher than that of solid Xe, an important factor for the initial stage of cluster formation on top of the buffer layer. To compare the growth of clusters formed on top of xenon or water as a buffer material, we used our results and the recently published data of Huang et al.¹⁹ and Haley et al.²⁰ Figure 6 summarizes $\langle n \rangle$ obtained by evaporation of 0.2 and ~ 1 Å of metal (Au and Ag) as a function of water and xenon buffer layer thickness (θ). $\langle n \rangle$ was found to be power law-dependent on θ , $\langle n \rangle \propto \theta^Z$, with $Z = -1.5$ for 0.2 Å of Ag and -2.3 for 1 Å of Au evaporated on top of the xenon buffer. Significantly smaller numbers are found when ASW is used as the buffer material with $Z = -0.45$ and -0.6 for the deposition of 0.2 and 1.2 Å of Au, respectively. It should be emphasized that the rate of deposition was the same in all experiments, within the range of 0.01–0.02 Å/s.

Using thin buffer layers (4–10 ML), the densities of clusters obtained with xenon as the buffer material are much higher than the densities obtained with water. Evaporation of 0.2 Å of metal on top of an ~ 5 ML buffer

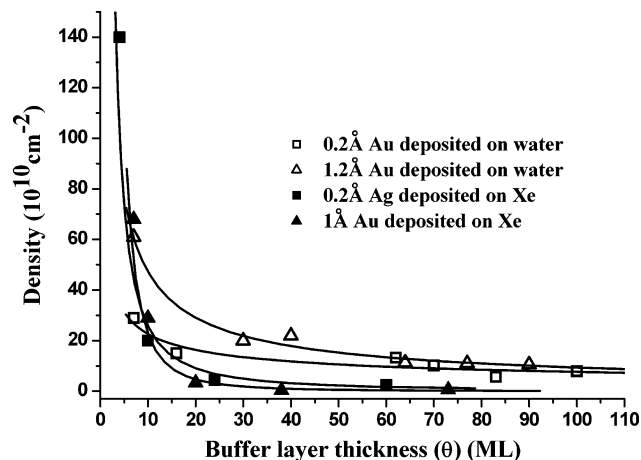


Figure 6. Comparison of the average density $\langle n \rangle$ of metallic (Au and Ag) clusters grown on xenon and on water as the buffer layers as a function of layer thickness for 0.2 and ~ 1 Å of evaporated metal. The data for Ag and Au deposited on Xe as the buffer layer were taken from refs 19 and 20. These authors employed room-temperature STM and TEM.

reveals a difference of more than an order of magnitude in density between xenon and water. This phenomenon can be understood in terms of the differences in the stiffness and heat capacity of the buffers. ASW layers are characterized by their hydrogen-bonded network of molecules, whereas the xenon atoms in the layer are held by the weaker van der Waals interactions. Consequently, water forms a stiffer layer. Moreover, the heat capacity of water is more than an order of magnitude larger than that of solid xenon. Thermally hot metal atoms deposited on top of the xenon buffer layer may penetrate into the buffer layer. Such a process has actually been described by Weaver and co-workers in an early work using photoemission to study the growth of metals on Xe/GaAs-(110).²³ The diffusion of metal atoms surrounded by xenon is expected to be slow and therefore limited to short distances. In contrast, hot metal atoms deposited on top of the stiffer and better heat-dissipating layer of ASW penetrate less into the molecular layer, if at all. Therefore, diffusion of the hot metal atoms on top of the ASW surface is expected to be faster, with less friction at the substrate interface. These small clusters, therefore, may diffuse longer distances, which is expected to result in more efficient cluster growth and faster aggregation. Consequently, smaller densities at thin buffer layers of ASW will form when compared to that of thin Xe layers, as experimentally observed.

Another point of interest is that the rate of change (decrease) in cluster density with increasing buffer layer thickness is much faster in the case of Xe than with water. Z values (power law) for the xenon layer are twice as large as those for the ASW buffer.

This experimental observation leads to the conclusion that the metal atoms or small clusters diffuse longer distances when the Xe layer desorbs, thus enhancing coalescence and aggregation. The faster diffusion rate into the layer can be understood as arising from the weak interatomic van der Waals attraction in the case of Xe, allowing metal clusters to pass through them more easily. Moreover, when clusters coalesce energy is released. This energy contributes to phonon excitation within the solid Xe layers. Consequently, the rate of aggregation is further enhanced.²¹ Water with its higher heat capacity dissipates heat efficiently; therefore, it is affected less by the released heat of coalescence.

Two processes control the growth of metallic clusters: atom diffusion on top of the buffer layer to form small seed clusters and diffusion of these small clusters during buffer desorption. When thin layers are used, the dominant process is the diffusion and clustering on top of the buffer layer. However, as the buffer layer becomes thicker the dominant step that dictates clusters density is the mobility of the metal clusters through the buffer layer upon its desorption. Therefore, in the case of thick enough buffer layers a faster diffusion rate of clusters through the xenon buffer would rapidly reduce the density via coalescence of small clusters, according to the BLAG mechanism.²¹ In contrast, slower diffusion rates of metal clusters through the water layer lead to smaller changes in the density of clusters as the buffer layer becomes thicker.

Differences in the height of clusters were also found between the two buffer materials. For 0.2 Å of evaporated metal on top of 60 ML, the average height is 3.0 and 1.2 nm for xenon and water buffers, respectively. Xenon as a buffer layer leads to clusters that are twice as high as clusters formed on top of ASW. This result can also be explained by the slower diffusion rate of clusters through the flux of the desorbing water layer. The fast diffusion rate through Xe is correlated nicely with the height of clusters because as the diffusion rate increases more clusters coalesce, inducing larger and therefore higher clusters.

3.6. BLAG versus Direct Deposition. The common method of metallic nanocrystal growth is the direct deposition of evaporated metal on solid surfaces and recently mostly on top of oxide substrates.^{1–4} The density and size of metallic clusters grown this way are functions of the substrate's temperature and amount or flux of evaporated metal.⁹ It is therefore interesting to make a comparison between direct and BLAG-grown clusters in terms of their size and density. We have carried out such a test on our SiO₂/Si(100) substrate. Gold clusters formed by the BLAG technique were prepared by evaporating 0.7 Å of Au on top of 40 ML of H₂O on the sample held at 140 K. The substrate was subsequently annealed to room temperature, which led to water desorption and to coalescence and growth of the metallic clusters. Directly deposited clusters were grown by evaporation of the same amount of gold on the bare SiO₂/Si(100) at room temperature.

The values obtained for $\langle n \rangle$ and $\langle h \rangle$ of directly deposited Au are $1 \times 10^{12} \text{ cm}^{-2}$ and $0.75 \pm 0.2 \text{ nm}$, respectively, whereas $\langle n \rangle$ and $\langle h \rangle$ obtained by the BLAG method were $1.5 \times 10^{11} \text{ cm}^{-2}$ and $1.8 \pm 0.9 \text{ nm}$, respectively. These results emphasize the significant differences in the growth modes of these two methods. Unlike the direct deposition procedure, the BLAG process enhances the diffusion and aggregation of clusters, which results in larger sizes on the account of reduced density.

Another important difference is the height distribution of the clusters. Clusters grown via the BLAG method on the SiO₂/Si(100) substrate are characterized by an average height distribution with a standard deviation of 50% after normalization, whereas clusters grown by direct deposition are more uniform with a standard deviation of only 25%. We conclude that the deposition of metal clusters assisted by buffer layers result in wider size distributions.

To verify the differences between clusters grown via the two methods, we have more carefully examined clusters formed by direct deposition and those grown via the BLAG method using 7 ML of H₂O. Limiting the buffer layer thickness to its lower value minimizes the aggregation step that characterizes the BLAG method.¹⁹ Therefore, variations in clusters size and density should reflect the

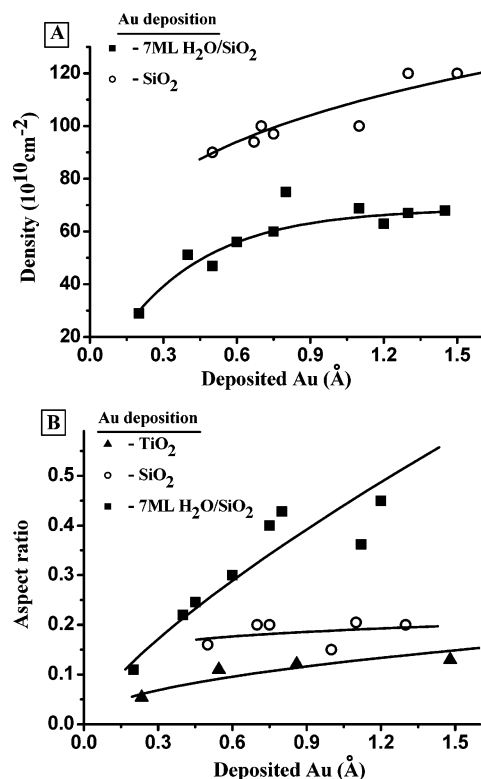


Figure 7. (A) Density of gold clusters as a function of the amount of deposited gold. The direct deposition of gold on a SiO₂ substrate is compared with the deposition of gold on top of 7 ML of water. (B) Aspect ratio (height/diameter) of gold clusters as a function of the amount of deposited gold for the same substrates as in A. In addition, we compare our results to the aspect ratio of gold clusters directly deposited on TiO₂, as reported by Kolmakov et al.¹⁴ The solid curves are a guide to the eye.

different diffusion rates and coalescence of the clusters on top of the oxide substrate (SiO₂) and those on the ASW layer. Densities of clusters obtained by direct evaporation are nearly twice as high as those obtained by the same $D_{(g)}$ values employing BLAG on ~ 7 ML of H₂O on top of our substrate (Figure 7A). In contrast, the average height of the clusters is almost doubled by employing the BLAG cluster growth procedure. For example, $\langle h \rangle$ has changed from 0.8 (direct deposition) to 2 nm (via BLAG on 7 ML of H₂O) for $D_{(g)} = 1.2 \text{ Å}$. Likewise, the aspect ratio (height/diameter) values of BLAG-grown clusters are typically twice as large (Figure 7B). A comparison between gold clusters grown by direct deposition on a TiO₂ substrate, as reported by Kolmakov et al.,¹⁴ and our results on a SiO₂ substrate reveals that the morphology of the clusters is similar despite the different oxide substrates. In both cases of direct deposition, the clusters have low aspect ratio values and only minor sensitivity of aspect ratio values to the amount of evaporated gold.

In conclusion, differences in density, height, and aspect ratio between clusters grown by the two methods suggest that the direct evaporation technique impedes the coalescence of small clusters on oxide surfaces at substrate temperature below 300 K. Furthermore, these clusters are characterized by a small aspect ratio and are therefore flatter and more 2D in nature than the BLAG-grown clusters. These differences suggest that the number and type of catalytically active sites on these clusters should be quite different in terms of yield and selectivity.

4. Conclusions

Water as a buffer layer for assisting the growth of gold nanocrystals has been studied.

The gold clusters grown in this work on SiO₂/Si(100) were examined by tapping mode AFM and HR-SEM to determine the aspect ratio of the clusters as a function of the water buffer layer thickness and the amount of evaporated gold. It was found that cluster size and density are power law-dependent on water layer thickness. An important aspect of this work has been a comparison of the shapes of clusters grown by direct deposition on the SiO₂ substrate and those made via the BLAG method.

We have shown that clusters grown by direct deposition are denser and flatter (small aspect ratio, more 2D-like) than BLAG clusters.

The role of the buffer material in cluster growth has been investigated as well. Different densities and aspect ratios determined for gold clusters grown on top of Xe and on water as the buffer materials were discussed in terms of heat capacity (the heat capacity of water is more than 10 times larger than the heat capacity of Xe) and stiffness (hydrogen bonding network in water) differences between the two buffer materials. The study of other molecular buffer materials with different heat capacities is in progress.

The larger aspect ratio of BLAG clusters compared to that of directly deposited clusters indicates a more 3D nature of the BLAG clusters. It is expected to result in more surface imperfections such as steps, kinks, and other low coordination number surface atoms. As was very recently pointed out on the basis of DFT calculations²⁸ and experimental data,²⁹ the high density of atoms with

low coordination numbers in the case of gold clusters in the size range of 2–4 nm is the key to the extraordinary CO oxidation activity of these clusters. We predict that enhanced activity of BLAG-grown gold clusters should be observed compared to the activity of those directly grown on oxide surfaces as far as CO oxidation is concerned. This, we speculate, should affect the catalytic activity of other transition-metal clusters and possibly their selectivity as well.

It was recently found that the density of clusters directly deposited on an oxide substrate is highly correlated to the defect density.³⁰ A future study should reveal whether one may bypass this dependence by employing the BLAG method. BLAG clusters softly land on the oxide substrate as small clusters and not as separate atoms; therefore, their diffusivity is expected to be limited compared to that of single metal atoms. This suggests a limited dependence on substrate defects upon preparation of metallic clusters employing the BLAG technique. Further investigation is needed to examine the stability of these water–BLAG clusters at elevated pressures and temperatures that are typical of industrial conditions.

Acknowledgment. This research was partially supported by a grant from the U.S.–Israel Binational Science Foundation and by the Israel Science Foundation. The Farkas center is supported by the Bundesministerium für Forschung und Technologie and the Minerva Gesellschaft für die Forschung mbh.

LA0512446

(29) Lemire, C.; Meyer, R.; Shaikhutdinov, S.; Freund, H. *J. Angew. Chem., Int. Ed.* **2003**, *43*, 118.

(30) Wallace, W. T.; Min, B. K.; Goodman, D. W. *J. Mol. Catal. A: Chem.* **2005**, *228*, 3.

(28) Lopez, N.; Janssens, T. V. W.; Clausen, B. S.; Xu, Y.; Mavrikakis, M.; Bligaard, T.; Nørskov, J. K. *J. Catal.* **2004**, *223*, 232.